Nonlinear dynamics of torsional waves in a drill-string model with spatial extent

David A.W. Barton, Bernd Krauskopf, and R. Eddie Wilson

28th February 2007

Abstract

In this paper we investigate the dynamics and bifurcations of an oil-well drill-string model that takes the form of a neutral delay differential equation (NDDE). We consider the torsional mode of the drill-string and investigate the associated stick-slip motion. To analyse the model we develop numerical continuation routines based on Fourier-methods since existing routines based on polynomial approximations are unable to cope with the presence of arbitrarily weakly damped modes. We find 'resonance peaks' in the dynamics where a high-frequency mode is superimposed on the underlying periodic behaviour causing large torsional waves in the drill-string. We show that the resonance peaks are robust to small perturbations in the friction parameters but disappear if static friction forces are neglected completely.

Keywords: delay differential equation, bifurcation, numerical continuation, Cosserat

1 Introduction and background

This paper presents a case study in advanced numerical techniques developed by the dynamical systems community and their application to mechanical engineering problems of real-world value. The specific problem that we consider is the modelling and analysis of stick-slip vibrations in oil-well drilling operations. Here surface machinery provides the torsional drive for a drill bit via a connecting shaft, known as a drill-string due to its high aspect ratio. One of the key problems in this type of drilling is the presence of torsional vibrations caused by nonlinear cutting forces and stick-slip interactions at the cutting face (Jansen, 1993).

The principal mathematical challenge concerns the spatial distribution of strain in the drill-string; many models use a simple lumped approximation where the deformation is modelled by a simple torsional spring (Jansen, 1991, 1993; van de Vrande, van Campen and de Kraker, 1999). This approach has been validated in laboratory experiments with relatively small aspect ratios (Mihajlović et al., 2004). However typical aspect ratios are far larger (Jansen, 1993). Similar models of this basic type also include regenerative effects at the cutting face (Germay et al., 2005), or a lumped lateral mode (Leine, van Campen and Keultjes, 2002) to account for effects such as whirl.

In contrast, we follow Tucker and Wang (1999*a*,*b*, 2003) and retain the full spatial distribution of strain. Tucker and Wang used the Cosserat theory of slender rods to derive a drill-string model that includes all of the features believed to be necessary for realism. The resulting model is a system of coupled partial differential equations (PDEs) which are then analysed through simulation. The complexity of their model means that other methods of analysis are not feasible.

Consequently, Balanov et al. (2003) derived a simplified model where the axial and radial modes of the drill-string are ignored, and a constant rotational driving velocity is prescribed. Their starting point is the linear torsional wave equation together with boundary conditions that model the constant driving velocity Ω at the top of the drill-string and the friction force and contact torque at the base. Under these conditions, the D'Alembert solution ansatz yields a model of the form

$$\dot{x}(t) = \dot{x}(t-2) + J^{-1}\left[F(x(t) - x(t-2) + \Omega) - x(t) - x(t-2) + \Omega\right], \tag{1}$$

which we analyse in this paper. Time has been rescaled such that the time taken for a wave to propagate from one end of the drill-string to the other is one (thus giving a time delay of two). Given a solution $x(t)$ to (1), the rotational velocity $\dot{\phi}(s,t)$ may be recovered as a function of time t and displacement s along the drill-string. Here J is a rescaled inertia parameter and the friction force F is given by

$$F(z) = -\frac{Az}{\sqrt{z^2+\varepsilon^2}}\left(1 + h\exp\left(-\Delta^{-1}\left(z^2+\varepsilon^2\right)^{\frac{1}{2}}\right)\right). \tag{2}$$

The right hand side of (1) features the delayed derivative term $\dot{x}(t-2)$ and so it is known as a neutral delay differential equation (NDDE). This transformation of a PDE with derivative boundary conditions to an NDDE is not uncommon; see for example (Barton, Krauskopf and Wilson, 2007; Blakely and Corron, 2004; Răsvan, Selişteanu and Niculescu, 2006; Stépán and Szabó, 1999). Generally, NDDEs present additional challenges over ODEs due to their infinite-dimensional phase space and the existence of delayed derivative terms. However, there is an additional difficulty with model (1): since the coefficient of the derivatives $\dot{x}(t)$ and $\dot{x}(t-2)$ are equal, its essential spectrum lies on the imaginary axis (see section 2). This degeneracy causes problems for numerical methods due to the existence of infinitely many, arbitrarily weakly damped modes.

In the core of their paper, Balanov et al. (2003) used simulation to study the long-time behaviour of (1) and found regions of parameter space, separated by bifurcations, where the dynamics are qualitatively distinct. The dominant behaviour consists of periodic stick-slip oscillations, where the drill bit becomes stuck (i.e., the rotational velocity at the base of the drill-string is zero) for a short time before the torque builds up sufficiently for the drill bit to be freed. They also showed the existence of tori and chaotic attractors, however, these occupy only small regions in parameter space. A typical series of velocity profiles along the length of the drill-string is shown in figure 1; the dashed line shows the (constant) rotational velocity at the top of the drill-string, the grey curves show the velocity at different points along its length, and the bold black curve shows the rotational velocity at the base of the drill-string. Note the region of slip-stick friction at the base of the drill-string where the rotational velocity is zero.

Since Balanov et al. used simulation as their sole investigative tool, they were only able to investigate parameter space at point values taken from a very coarse grid in two parameters (the driving torque Ω and magnitude of the friction A; see for example (Balanov et al., 2003, Fig. 4)). Furthermore, the slow relaxation times of the periodic orbits and other attractors mean that it is computationally expensive to reach steady-state by long-time simulations. Consequently, much of the relevant dynamical behaviour of (1) has been missed so far.

In this paper, we develop numerical continuation techniques based on Fourier methods in order to investigate the dynamics and bifurcations of the NDDE model (1) as detailed in section 2. Through our analysis in section 3 we find undesirable motions in the form of 'resonance peaks' — high-frequency oscillations that were overlooked by the original investigation. These high-frequency oscillations are superimposed on the fundamental periodic behaviour of the dynamics resulting in regions of high torque, where torsional waves travelling along the

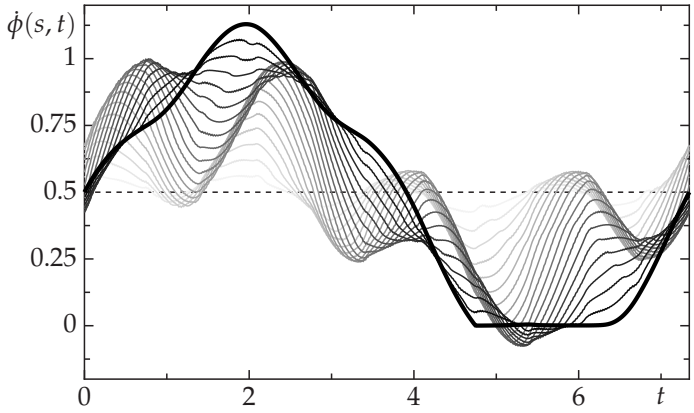

Figure 1: The rotational velocity of the drill-string along its length. The shade of grey indicates the position along the length; the bold black curve is the rotational velocity at the base of the drill-string and the dashed line is the (constant) rotational velocity at the top of the drill-string.

drill-string interact in an additive way. Consequently, operation in these parameter regimes could lead to damage of the drill-string. In section 4, we perform a sensitivity analysis of the friction parameters and we show that under small perturbations, the dynamics remains qualitatively unchanged. In particular, the resonance peaks persist although their amplitude is diminished if the static friction effects are reduced. We conclude in section 5 with remarks on possible future directions of research.

2 Computational methodology

We use numerical continuation as the principal tool for investigating the global dynamics of (1). This allows us to find and follow equilibria and periodic solutions in the system parameters, and to locate bifurcations. The fundamental idea is that the implicit function theorem guarantees the (local) existence of a solution branch which can be traced out with a predictor-corrector approach. The stability of solutions on the branch can then be found via eigenvalues of equilibria or Floquet multipliers of periodic orbits, respectively. Consequently, local bifurcations (e.g., Hopf and fold bifurcations) can be detected and can then in turn be continued in two parameters by appending test functions to the system definition. For a general introduction to continuation methods see (Doedel, Keller and Kernevez, 1991*a*,*b*; Kuznetsov, 1998; Seydel, 1994). Software has been available for the continuation of ODEs for many years in the form of AUTO (Doedel et al., 1998) and MATCONT (Dhooge et al., 2006). However, packages that continue solutions of DDEs are comparatively new (Engelborghs, Luzyanina and Samaey, 2001; Szalai, 2005) and extensions to deal with NDDEs even more so (Barton, Krauskopf and Wilson, 2006).

The chief technical difficulty here is that delay differential equations (DDEs) define infinite dimensional dynamical systems (Diekmann et al., 1995; Hale and Verduyn Lunel, 1993; Kolmanovskii and Myshkis, 1999; Kuang, 1993; Stépán, 1989) since their initial data must be prescribed over the delay interval $t \in [-\tau, 0]$ to give a unique solution. Note that for standard DDEs without neutral delay terms, there can only be a finite number of eigenvalues to the right of any vertical line in the complex plane (Hale and Verduyn Lunel, 1993) and, hence, the stability arguments and bifurcations are predominantly the same as for ODEs. However, for NDDEs, the eigenvalues may accumulate on vertical lines in the complex plane where the *essential spectrum*, which is due to the delayed derivative term, is located. Consequently

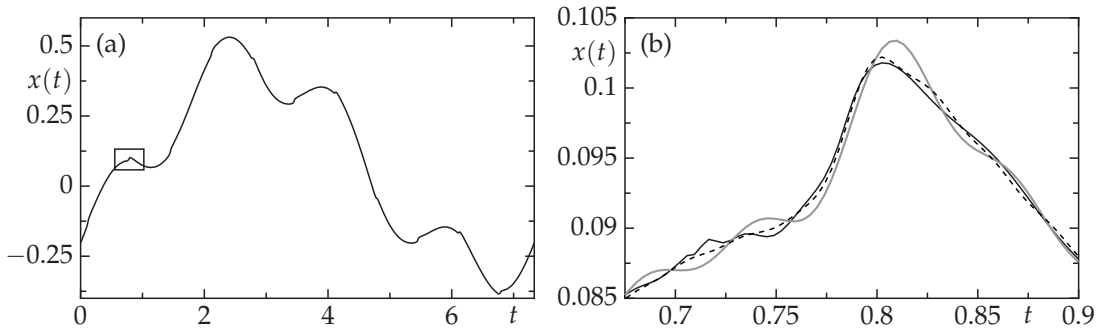

Figure 2: A comparison of a periodic orbit computed using 256 (grey curve), 512 (dashed curve), and 1024 (solid curve) Fourier modes. The right-hand panel shows an enlargement of part of the orbit.

'infinite-dimensional' bifurcations may occur where the essential spectrum passes through the imaginary axis. This effect can give rise to non-smooth periodic orbits (Engelborghs and Roose, 1999), which are possible even in NDDEs with smooth nonlinearities because a gradient discontinuity at $t = 0$ is propagated by the delayed derivative term (Hale and Verduyn Lunel, 1993).

In general the essential spectrum is located by considering the eigenvalues of the difference equation associated with the NDDE (Hale and Verduyn Lunel, 1993), namely $x(t) - x(t-\tau) = 0$ for (1). This argument shows that (1) is degenerate: exponential stability is impossible, because the essential spectrum is located on the imaginary axis. Furthermore, the presence of modes with arbitrarily high frequency and weak damping causes numerical stability problems. We would expect more sophisticated drill-string models to include dissipation in the torsional wave equation thus alleviating these difficulties.

In order to continue the periodic orbits of (1), we must implement a suitable numerical discretisation. The standard approach is to use the method of collocation with orthogonal polynomials (Doedel, Keller and Kernevez, 1991*b*) where a piecewise polynomial is sought that satisfies the differential equation at discrete values of the independent variable known as the *collocation points*. This approach produces a large system of algebraic equations which can be fed to standard nonlinear solvers.

For (1) we have found that this collocation method fails, because the high-frequency weakly-damped modes prevent the nonlinear solver from converging unless the predicted solution is extremely close to the true solution. To make collocation work, one must either (i) use several thousand collocation points, which makes the computation extremely expensive; or (ii) work on an approximate problem where the coefficient of the delayed derivative term is reduced to less than one so that eigenvalues are bounded away from the imaginary axis. The latter approach may induce spurious dynamics.

In this paper we abandon collocation polynomials and instead use a Fourier-based collocation method, which truncates high frequencies. We discretise the periodic orbit $x(t)$ at equispaced mesh points such that $u_i = x(t_i)$. In order to work solely in the time domain, we use a Fourier differentiation matrix D to calculate derivatives (i.e., $\dot{x}(t_i) = Du$) and an interpolation matrix I_n to calculate the delayed terms (i.e., $x(t_i - \tau) = I_n u$). The Fourier differentiation and interpolation matrices are formed using the methods described in (Weideman and Reddy, 2000). The substitution of these terms into (1) produces a large system of nonlinear algebraic equations which can be solved using standard techniques.

For (1) this Fourier-based method is far superior to the corresponding scheme based on orthogonal polynomials, although the difference between the methods for other problems is

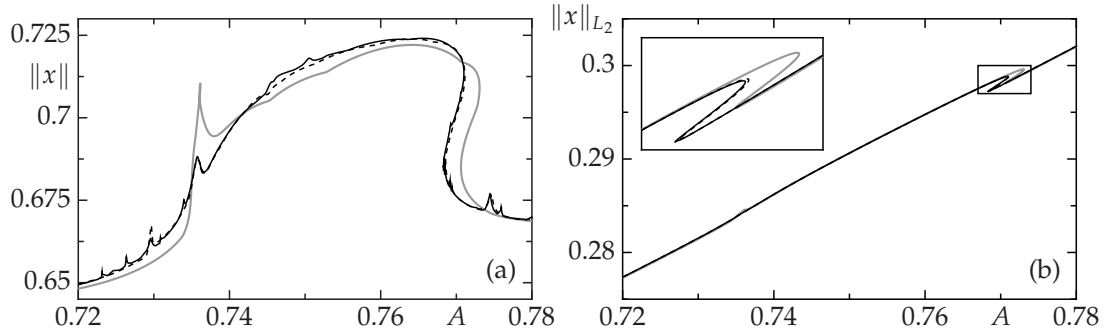

Figure 3: A comparison of a branch of periodic orbits computed using 256 (grey curve), 512 (dashed curve), and 1024 (solid curve) Fourier modes. The left-hand panel shows a projection using the max-min solution measure (3) and the right-hand panel shows a projection using the L_2-norm (4).

often not so clear cut. For a crude approximation to a periodic orbit, we typically require 256 Fourier modes whereas the orthogonal polynomial method requires in the order of 4000 mesh points simply to converge. Figure 2 examines the convergence of a computed periodic orbit as the number of modes is increased. When using 1024 modes, the Fourier solution is indistinguishable from that computed via simulation of the initial value problem. However, 256 Fourier modes is sufficient for most purposes — differences only become apparent on close inspection of the orbits.

We now examine the convergence of branches of periodic solutions computed with different numbers of modes; see figure 3. This comparison uses the max-min (pseudo-) norm

$$\|x\| = \max x(t) - \min x(t), \tag{3}$$

and the more common L_2-norm

$$\|x\|_{L_2} = \left(\int_0^1 x^2(Tt) \mathrm{d}t \right)^{\frac{1}{2}}, \tag{4}$$

where T is the fundamental period. The max-min norm shows that much of the fine detail of the branches with 512 and 1024 Fourier modes is missing from the branch with 256 Fourier modes. Furthermore, the location of the fold bifurcation in the branch is slightly different when using 256 Fourier modes. There is little difference between the branches when viewed with the L_2-norm (figure 3(b)) and since it obscures most of the fine detail, we use the max-min norm throughout the remainder of the paper.

3 Numerical continuation study

We now investigate the dynamics of (1) with the numerical continuation method described in section 2. We concentrate on the parameter regime identified by Balanov et al. (2003) as the most physically relevant, namely $0 \leq \Omega \leq 1$, $0 \leq A \leq 1$, $J = 1$, $h = 0.2$, $\Delta = 0.1$, $\varepsilon = 0.001$. Balanov et al. summarise the (predominantly periodic) dynamics of (1) in the (Ω, A)-plane with the help of a two-parameter bifurcation diagram (Balanov et al., 2003, Fig. 4). This diagram was produced by a series of long-time simulations on a 25×25 point grid in parameter space. The coarseness of this grid obscures much of the detailed structure of the dynamics and misses some of the key behaviour that we find here.

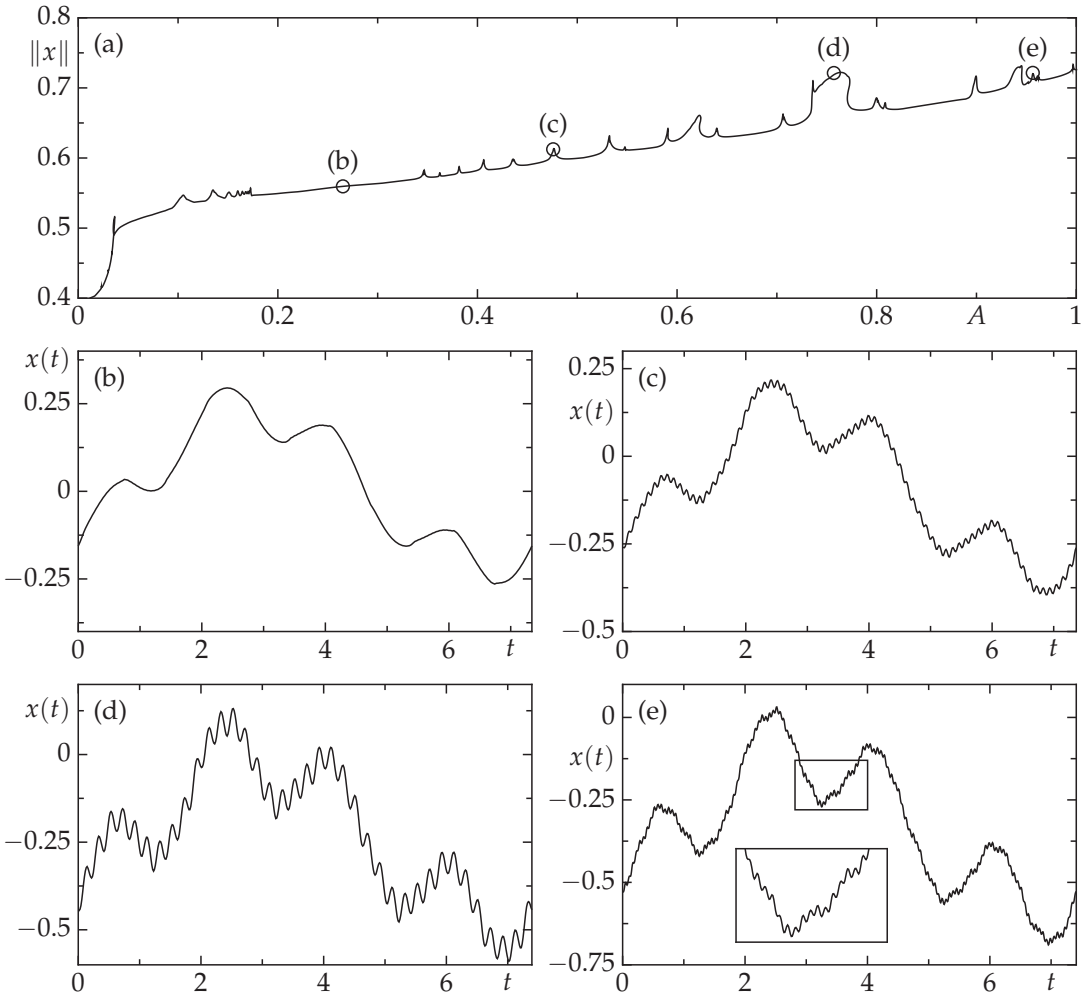

Figure 4: A branch of stable periodic orbits of (1) for $0 \leq A \leq 1$ and $\Omega = 0.3$ (a). Representative periodic orbits (c)–(e) are shown, which have different high-frequency modes superimposed on the 'basic' periodic orbit (b).

To begin our investigation we require a starting solution of (1), which we obtain using numerical simulation of the initial value problem with the software package RADAR5 (Guglielmi and Hairer, 2001, 2005*a*,*b*), which is specifically designed for stiff DDE/NDDE systems. Once a starting solution has been obtained, numerical continuation allows us to do away with simulation and consider the long-time dynamics directly along with any unstable dynamics.

We start with figure 4(a), a one-parameter continuation for fixed $\Omega = 0.3$, which shows a branch of periodic orbits with their min-max norm (3) plotted against A. A representative time profile of an attracting periodic orbit is shown in figure 4(b) for $A = 0.265$. As A is increased from zero, there is a sudden increase in $\|x\|$ at $A \approx 0.035$; this corresponds to the onset of stick-slip effects at the base of the drill-string. When A is increased further, a series of peaks can be seen along the branch; the periodic orbits at the tips of these peaks show strong resonant behaviour, i.e., there is a secondary high-frequency mode superimposed on the period one behaviour — see for example figures 4(c)–(e). The existence of these resonance peaks is not mentioned in (Balanov et al., 2003) and was probably missed due to the coarseness of their (A, Ω)-parameter grid. Figure 5(a) shows an enlargement of a single peak in the branch shown in figure 4(a). From the time series in figures 5(b)–(d) we see that the amplitude of the

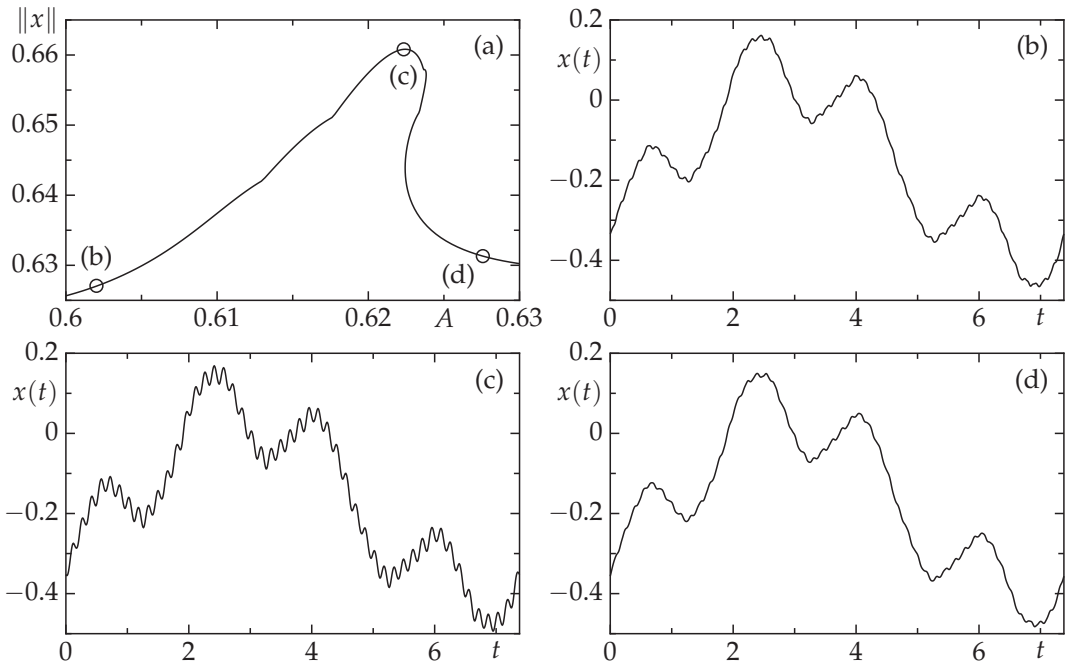

Figure 5: A solution branch (a) and a series of periodic orbits (b)–(d) showing the effect of increasing A through a resonance peak for $\Omega = 0.3$. Panels (b) and (d) show that away from the peak there is small scale oscillatory behaviour, and panel (c) shows that at the peak this oscillatory behaviour is pronounced.

secondary frequency grows until the tip of the peak and then continuously decreases again as the vicinity of the peak is left. Note that the resonance peak shown in figure 5(a) undergoes a pair of fold bifurcations, resulting in a hysteretic loop with a small region of bistability. Hysteretic loops similar to this are seen in the vicinity of many of the resonance peaks found in (1).

The secondary frequency seen in the periodic orbit changes from peak to peak, as can be seen by comparing figures 4(c)–(e). Overall the periodic orbit changes very little along the branch, although a large variation in the secondary frequencies is found (compare figures 4(d) and (e)). There appears to be a strong correspondence between the secondary frequency and the size of the peak, both in terms of $\|x\|$ and the range of A for which it occurs — the lower frequencies result in higher values of $\|x\|$ and occur over a larger range of A. With this in mind, it can be seen from figure 4(a) that there is no immediately apparent pattern in the occurrence of the different frequencies. Note that in the vicinity of (b) in figure 4(a) ($0.2 \leq A \leq 0.3$) there are no peaks appearing on the branch. However, when this portion of the branch is recomputed with 1024 Fourier modes, new peaks appear, whose frequencies are too high to be found with the lower number of (256) Fourier modes used originally. Due to the computational effort involved and the otherwise good convergence properties, we have decided to calculate all the solution branches with the lower number of Fourier modes. Thus we accept that some of the (very) high-frequency behaviour will be missed.

To understand the behaviour of the drill-string at resonance peaks, we must first transform the periodic orbits into rotational velocities along the length of the drill-string. Figure 6 shows the rotational velocities and resultant torques at two points along the drill-string for the periodic orbits found in figures 4(d) and (e). At the base of the drill-string (in figures 6(a1) and (a2)) the secondary frequency is not apparent in the velocity profile, although it can be seen in the resultant torque (in figures 6(b1) and (b2)). This is because the secondary frequency is

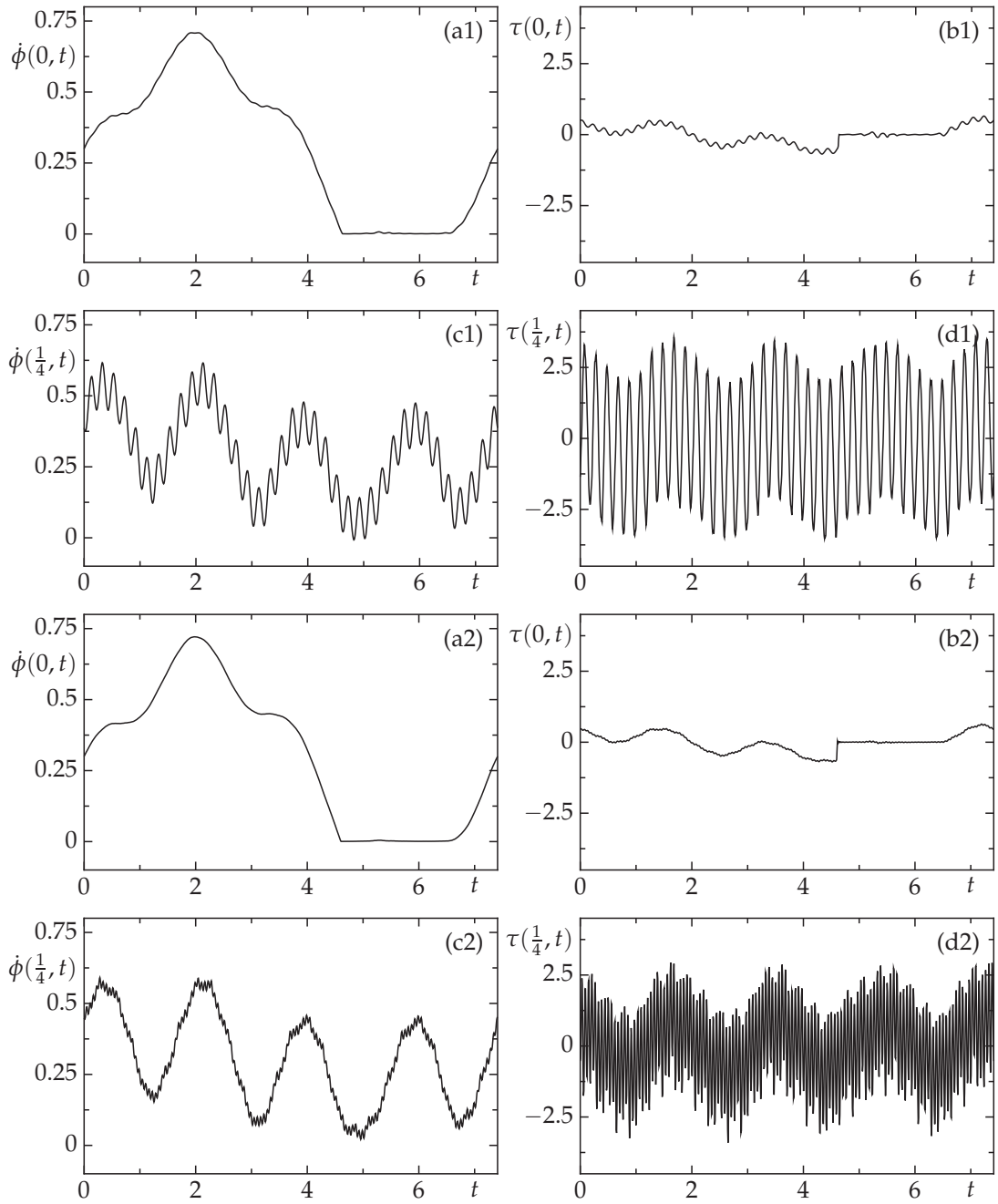

Figure 6: A series of velocity $\dot{\phi}$ and resultant torque τ profiles corresponding to the solutions shown in figures 4(d) and (e) respectively. Panels (a1) and (a2) show the velocity profile at the base of the drill-string where the secondary frequency is cancelled out (the corresponding torque profiles are shown in (b1) and (b2)). Also, note the regions of slip-stick behaviour where the velocity is close to zero. Panels (c1) and (c2) show the velocity profile a quarter of the way up the drill-string where the secondary frequency is clearly seen (again, corresponding torque profiles are shown in (d1) and (d2)).

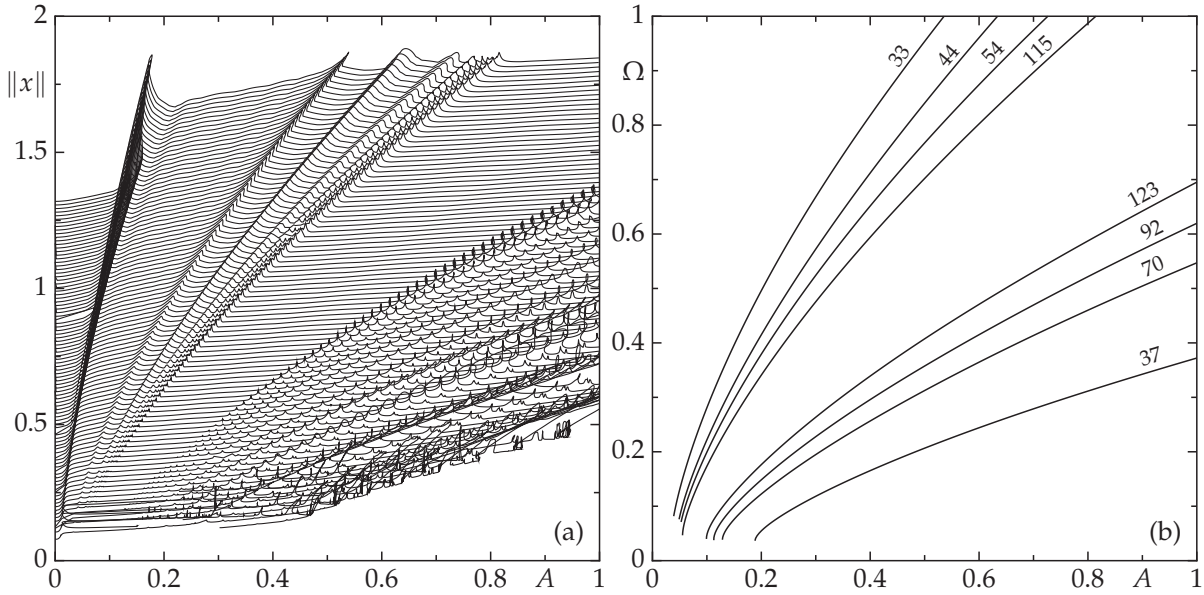

Figure 7: (a) A waterfall diagram made from a series of one-parameter continuations in A for $h = 0.2$ and $0.05 \leq \Omega \leq 1$, in increments of 0.01, plotted against $\|x\|$. The top-most branch corresponds to $\Omega = 1$ and the bottom-most branch corresponds to $\Omega = 0.05$. The evolution of the resonance peaks can be traced through parameter space. Note that the higher frequency resonance peaks are missing since only 256 Fourier modes are used. (b) Several of two-parameter continuations along branches of constant period. Each branch corresponds to a resonance ridge. The number associated with each branch is the number of secondary oscillations per period. The continuations are stopped when the secondary oscillations are no longer present.

commensurate with the delay time and the velocity at the base of the drill-string is given by $\dot{\phi}(0,t) = x(t) - x(t-2) + \Omega$; i.e., the secondary frequency is cancelled out. At other points along the drill-string however, the effect of the secondary frequency can be magnified via the same mechanism. Figures 6(c1) and (c2) show the velocity a quarter of the way up the drill-string and here the effect of the secondary frequency is pronounced. Furthermore, the resultant torques created in the drill-string at this location are about five times larger than those at the base and thus may prove damaging to the structure.

To build up a picture of the dynamics across the whole of the parameter plane $0 \leq A \leq 1$ and $0 \leq \Omega \leq 1$, we perform a series of one-parameter continuations in A for fixed $0.05 \leq \Omega \leq 1$ in increments of 0.01. The result is shown as a waterfall diagram in figure 7(a), plotted with A against $\|x\|$. The top branch corresponds to $\Omega = 1$ and the bottom one to $\Omega = 0.05$. This figure shows that the resonance peaks are not isolated but rather form ridges in the (A, Ω)-parameter plane, along each of which the secondary frequency remains constant and the period of the orbits changes very little. In figure 7(b) we show a few two-parameter continuations where the period of the orbit is kept constant. These branches trace out the ridges of resonance peaks and the number of secondary oscillations per period is labelled on each branch. The branch continuation is stopped when the secondary oscillations are no longer visible in the solution profiles.

All of the ridges appear to 'fan out' from the origin of the parameter plane and grow in magnitude. This behaviour is reminiscent of Arnold tongues of the circle map (Rasband, 1990) where, at particular points in parameter space, the dynamics are governed by phase-locked tori

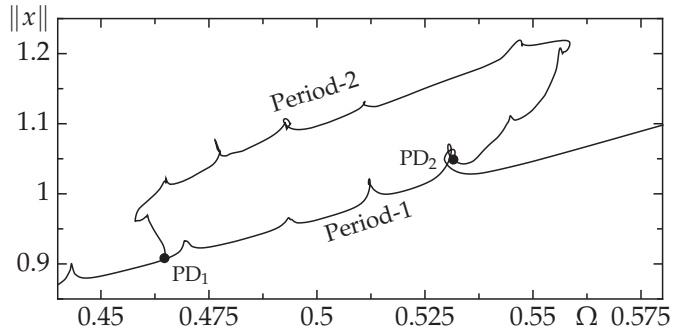

Figure 8: A one-parameter continuation in Ω for $A = 0.7$ showing the period-one branch and the bifurcating period-two branch. The period-two branch shows similar resonance peaks.

(different parameter choices result in different frequencies). Here, the periodic orbits do not lie on a torus but the effect is similar; within each of the resonance peaks there is phase-locking-like behaviour with the secondary frequency commensurate to the fundamental frequency of the orbit. The extent of this similarity is not yet known but may prove to be an interesting avenue for future research.

Balanov et al. (2003) note that there are a number of different stable attractors in the (A, Ω)-plane. These include period-doubled orbits, tori, and chaotic attractors. Here we restrict ourselves to the purely periodic behaviour and find accurate boundaries for the period-doubled orbits. In figure 8 we show a one-parameter continuation in Ω for $A = 0.7$ where the main branch of periodic orbits undergoes two subcritical period-doubling bifurcations, PD_1 and PD_2. The emerging period-two branch becomes stable after the folds, resulting in a small region of bistability between the period-one and period-two orbits. It can be seen that the period-two branch has similar resonance peaks to the period-one branch. Note that, although one of the period-doubling bifurcations appears to coincide with one of the resonance peaks, this is generally not the case. We continue the period-doubling bifurcations in two parameters to find the domain of existence of the period-two orbits by appending suitable test functions to (1) and by allowing a second parameter to vary (in this case A); see (Kuznetsov, 1998, Chapter 10). The results are shown in figure 9(a) and the period-two orbits can be seen to exist in a small wedge of parameter space.

When A is large and Ω is small, no periodic orbits are found at all, and the stable attractors are either chaotic or quasi-periodic. One-parameter continuations indicate that the periodic orbits disappear at a fold bifurcation. In a similar way to the continuation of period-doubling bifurcations it is also possible to continue fold bifurcations in two parameters. Thus, in figure 9 we also show the region bounded by fold bifurcations where no periodic orbits exist (labelled "No P.O.s"). This region corresponds to the bottom right-hand corner of figure 7(a).

Figure 9 represents a vast improvement on the bifurcation diagram shown in (Balanov et al., 2003, Fig. 4). Thus, we conclude that continuation methods allow (1) to be investigated far more effectively than is possible with simulation alone.

4 Sensitivity analysis for friction parameters

Balanov et al. (2003) consider the variation of the parameters A and Ω only. However, it is also important to know how sensitive the dynamics are to changes in the details of the friction law, since in the real world its precise form is uncertain. Figure 10 shows a schematic diagram of the shape of the friction function $F(z)$ used here; roughly speaking ε controls the slope at 0, h

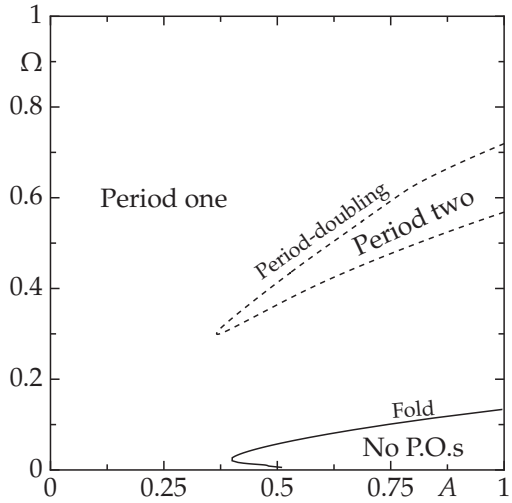

Figure 9: A two-parameter bifurcation diagram in the (Ω, A)-plane showing the domain of existence of period-doubled orbits (the dashed line denotes a curve of period-doubling bifurcations). In the region enclosed by the solid curve (a fold bifurcation curve) there are no periodic orbits in existence. The dynamics of this region are dominated by tori and chaotic attractors.

is the overshoot due to static friction, Δ is the characteristic width of the overshoot, and A is the overall amplitude.

We start by considering the effect of changing h. Figure 11(a) shows a waterfall diagram computed for $h = 0.1$, cf., figure 7(a). An initial comparison of the two figures shows that the main features of the branches are preserved and, in particular, the resonance peaks persist. However, resonance peaks for $h = 0.1$ are far less prominent than for $h = 0.2$, indicating that they result from the overshoot in the friction law. On closer examination, it appears that figure 11(a) is a scaling of figure 7(a), i.e., there is a high degree of similarity between the branches for $0 \leq A \leq 1$, $0 \leq \Omega \leq 1$, $h = 0.1$ and those for $0 \leq A \leq 0.5$, $0 \leq \Omega \leq 1$, $h = 0.2$. This suggests that there is an approximate scaling law involving A, Ω, and h that gives the location of the resonance peaks. The relationship becomes even clearer when we compare the constant period branches (the resonance ridges) in the (A, Ω)-plane for $h = 0.2$ (figure 7(b))

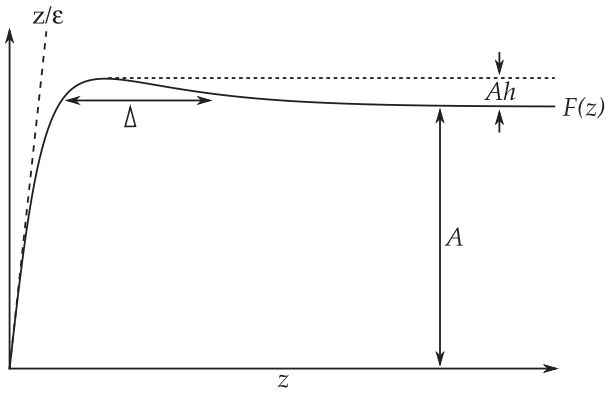

Figure 10: A schematic of the friction force F and the parameters governing its shape: ε controls the derivative of F at 0, h is the overshoot associated with static friction effects, Δ is the characteristic width of the overshoot, and A is the overall amplitude of F.

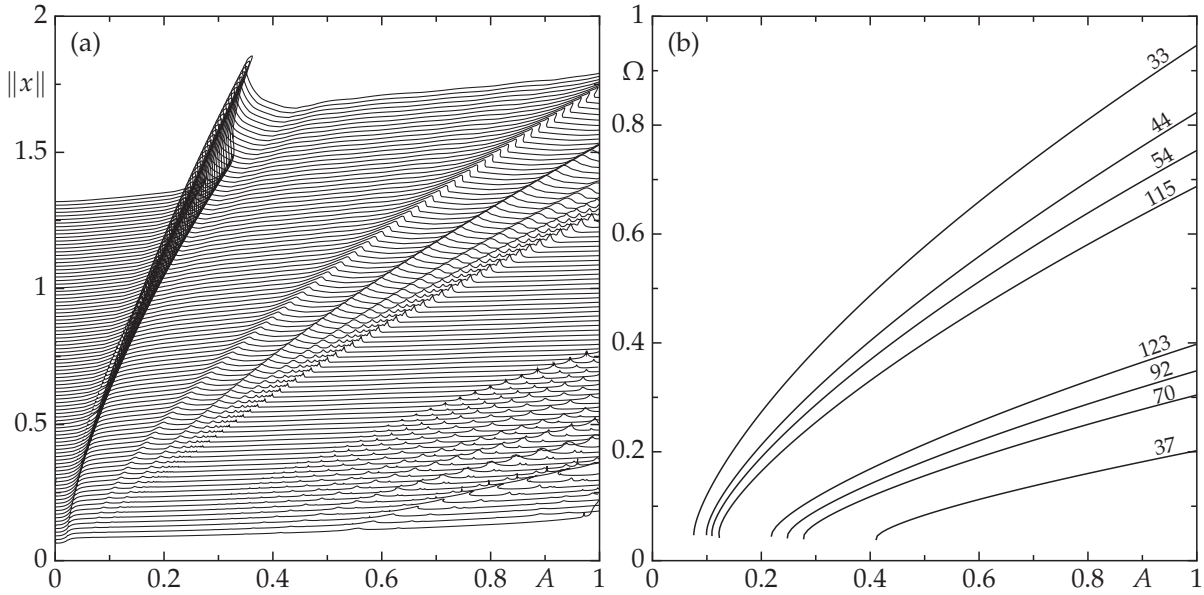

Figure 11: (a) A waterfall diagram made from series of one-parameter continuations in A for $h = 0.1$ and $0.02 \leq \Omega \leq 1$, in increments of 0.01, plotted against $\|x\|$. The top-most branch corresponds to $\Omega = 1$ and the bottom-most branch corresponds to $\Omega = 0.02$. The resonance peaks are far less pronounced in comparison with figure 7. (b) Two-parameter continuations of the resonances ridges shown in panel (a). The continuations are stopped when the secondary oscillations are no longer present. The numbers indicate the number of secondary oscillations per period.

and for $h = 0.1$ (figure 11(b)). However, the precise functional form of the scaling is currently unknown.

We also find for $h = 0.1$ that there are no period-doubled orbits in the region $0 \leq A \leq 1$, $0 \leq \Omega \leq 1$ and the period-one orbit covers the whole parameter plane (i.e., the period-one orbit does not disappear at a fold bifurcation). Consequently, the overshoot h in the friction law appears to cause much of the high frequency behaviour in the system. In the case that the friction function is monotone (i.e., $h = 0$) no slip-stick behaviour occurs and, correspondingly, no periodic behaviour can be found in the system — all of the dynamics are either quasi-periodic or chaotic.

We now consider the effect of changing the width Δ of the overshoot in F. In figure 12 we show the constant period branches that correspond to particular secondary frequencies for $\Delta = 0.2$; compare with figure 7(b) for $\Delta = 0.1$. (Note that the period of the respective branches changes when Δ changes.) There are no significant qualitative differences between $\Delta = 0.1$ and $\Delta = 0.2$. Furthermore, when a waterfall diagram (like figure 7(a)) is computed for $\Delta = 0.2$, the picture changes very little (the amplitudes and positions of the resonance peaks alter slightly) and consequently we do not show the figure here. It seems that changes in h and Δ have very similar effects; they scale the parameters for which resonance peaks exist, albeit nonlinearly.

Our investigations show that the remaining parameter ε appears to change the structure of the branches very little, far less than changes in h and Δ and so we do not consider this parameter to be of importance. Consequently, small changes to the friction parameters Δ, h, and ε do not result in any qualitative change to the dynamics. Furthermore, the quantitative changes that do occur appear to be related by a scaling of the friction parameters.

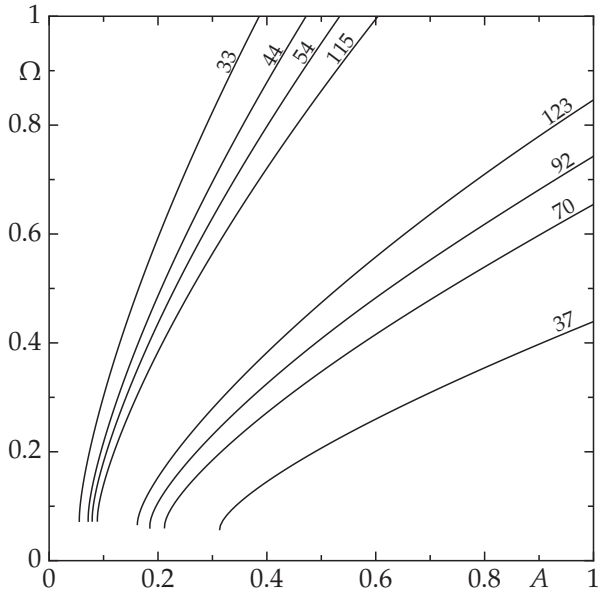

Figure 12: A two-parameter continuations of the resonances ridges shown for $h = 0.2$, $\Delta = 0.2$. The continuations are stopped when the secondary oscillations are no longer present. Compare with figures 7(b) and 11(b).

5 Conclusions

In this paper we have shown that numerical continuation is a powerful method for understanding the global dynamics of the drill-string model (1) proposed by Balanov et al. (2003). However, standard continuation software based on collocation with orthogonal polynomials cannot be used due to the presence of arbitrarily weakly damped modes. Instead we developed a new Fourier-based collocation method for NDDEs, which enables us to truncate the high-frequency modes that cause numerical problems. Collocation-based methods have the advantage over numerical simulation since the long-term dynamic behaviour is found directly, without the need for lengthy simulation runs to eliminate transient behaviour. Furthermore, unstable orbits can be found and continued without difficulty.

Numerical continuation of (1) revealed that important dynamical effects were missed in the original study (Balanov et al., 2003). Specifically, we have found resonance peaks (ridges in the two-parameter plane) where a secondary high-frequency mode is superimposed on an underlying periodic orbit exhibiting stick-slip motion. While these secondary modes have very little effect at the base of the drill-string, they can cause large torsional waves to propagate through the drill-string. Furthermore, with numerical continuation we were able to perform a sensitivity analysis for the friction parameters. The dynamics of (1) were found to be qualitatively equivalent under small perturbations from the parameter set chosen by Balanov et al. (2003). The quantitative changes we found relate entirely to the modelling of the static friction force, namely the parameters h and Δ. We found that decreasing h or Δ produces a decrease in the amplitude of the secondary oscillations associated with the resonance peaks. When these parameters are decreased sufficiently, stick-slip motion ceases. Furthermore, when the friction force law becomes monotonic periodic behaviour disappears entirely, leaving only quasi-periodic and chaotic motion.

The presence of the resonance peaks in the solutions of (1) draws into question its validity as a model for drill-string dynamics. The high-frequency secondary modes appear to be a direct result of the degeneracy of (1) that its essential spectrum lies on the imaginary axis. In

practise the existence of infinitely many weakly damped, high-frequency modes is unrealistic; rather we would expect the high-frequency oscillations to be damped out through dissipative effects in the drill-string. Thus, a future extension to the model could be to include a dissipative term in the drill-string's torsional wave equation. Damping effects are also important in the consideration of the friction force, which here is a smooth function whereas many models in the literature incorporate a discontinuity at zero. See for example the friction models used in (Germay et al., 2005; Leine, van Campen and Keultjes, 2002). Since the delayed derivative term in (1) has a coefficient of one, gradient discontinuities caused by the friction function would be propagated forward in time without decay.

One final consideration for the future is the need for a comparison of the ODE models used in (Jansen, 1991, 1993; van de Vrande, van Campen and de Kraker, 1999) with the NDDE/PDE models in (Balanov et al., 2003; Tucker and Wang, 1999*a*,*b*, 2003), at realistic parameter values. Such a comparison is needed to determine the importance of the spatial behaviour that is present in the NDDE/PDE models but missing from the ODE models.

This paper has shown that numerical continuation methods for NDDEs are ready to be applied to real-world challenges such as those arising from the full drill-string model of Tucker and Wang (1999*a*,*b*) where the radial and lateral modes are also included. Further examples arise in the field of dynamic substructuring/hybrid testing (Kyrychko et al., 2006) where numerical and physical experiments are coupled together in real-time. The principal challenge that remains for the development of a general continuation tool for NDDEs is to understand the bifurcations that can occur when the essential spectrum passes through the imaginary axis.

References

Balanov, A.G., Janson, N.B., McClintock, P.V.E., Tucker, R.W., and Wang, C.H.T., 2003, "Bifurcation analysis of a neutral delay differential equation modelling the torsional motion of a driven drill-string," *Chaos, Solitons & Fractals* 15(2), 381–394.

Barton, D.A.W., Krauskopf, B., and Wilson, R.E., 2006, "Collocation schemes for periodic solutions of neutral delay differential equations," *Journal of Difference Equations and Applications* 12(11), 1087–1101.

Barton, D.A.W., Krauskopf, B., and Wilson, R.E., 2007, "Homoclinic bifurcations in a neutral delay model of a transmission line oscillator," *Nonlinearity* 20(4), 809–829.

Blakely, J.N., and Corron, N.J., 2004, "Experimental observation of delay-induced radio frequency chaos in a transmission line oscillator," *Chaos* 14(4), 1035–1041.

Dhooge, A., Govaerts, W., Kuznetsov, Y.A., Mestrom, W., Riet, A.M., and Sautois, B., 2006, *MATCONT and CL_MATCONT: Continuation toolboxes in Matlab*, `http://www.matcont.ugent.be/`.

Diekmann, O., van Gils, S., Lunel, S.M.V., and Walther, H.-O., 1995, *Delay equations: functional, complex, and nonlinear analysis,* vol. 110 of *Applied Mathematical Sciences*, Springer, New York.

Doedel, E.J., Champneys, A.R., Fairgrieve, T.F., Kuznetsov, Y.A., Sandstede, B., and Wang, X., 1998, *AUTO 97: continuation and bifurcation software for ordinary differential equations*, `http://indy.cs.concordia.ca/auto/`.

Doedel, E.J., Keller, H.B., and Kernevez, J.P., 1991*a*, "Numerical analysis and control of bifurcation problems, part I," *International Journal of Bifurcation and Chaos* 1(3), 493–520.

Doedel, E.J., Keller, H.B., and Kernevez, J.P., 1991*b*, "Numerical analysis and control of bifurcation problems, part II, " *International Journal of Bifurcation and Chaos* 1(4), 745–772.

Engelborghs, K., Luzyanina, T., and Samaey, G., 2001, DDE-BIFTOOL v. 2.00: a Matlab package for bifurcation analysis of delay differential equations, Technical Report TW330, Department of Computer Science, K.U. Leuven, Leuven, Belgium.

Engelborghs, K., and Roose, D., 1999, "Smoothness loss of periodic solutions of a neutral functional-differential equation: on a bifurcation of the essential spectrum, " *Dynamics and Stability of Systems* 14(3), 255–273.

Germay, C., van de Wouw, N., Sepulchre, R., and Nijmeijer, H., 2005, "Axial stick-slip limit cycling in drill-string dynamics with delay, " in *Proceedings of ENOC-2005,* Eindhoven, Netherlands.

Guglielmi, N., and Hairer, E., 2001, "Implementing Radau IIA methods for stiff delay differential equations, " *Computing* 67(1), 1–12.

Guglielmi, N., and Hairer, E., 2005*a*, "Automatic computation of breaking points in implicit delay differential equations, " preprint, Università dell'Aquila, Italy.

Guglielmi, N., and Hairer, E., 2005*b*, Users' guide for the code RADAR5 - version 2.1, technical report, Università dell'Aquila, Italy.

Hale, J.K., and Verduyn Lunel, S.M., 1993, *Introduction to functional differential equations,* number 99 *in* "Applied Mathematical Sciences", Springer.

Jansen, J.D., 1991, "Non-linear rotor dynamics as applied to oilwell drillstring vibrations, " *Journal of Sound and Vibration* 147(1), 115–135.

Jansen, J.D., 1993, Nonlinear dynamics of oilwell drillstrings, PhD thesis, Delft University of Technology.

Kolmanovskii, V., and Myshkis, A., 1999, *Introduction to the theory and applications of functional differential equations,* Kluwer Academic Publishers, Dordrecht.

Kuang, Y., 1993, *Delay differential equations with applications in population dynamics,* number 191 *in* "Mathematics in science and engineering, " Academic Press, Boston.

Kuznetsov, Y.A., 1998, *Elements of applied bifurcation theory,* number 112 *in* "Applied Mathematical Sciences, " 2nd ed., Springer, New York.

Kyrychko, Y.N., Blyuss, K.B., Gonzalez-Buelga, A., Hogan, S.J., and Wagg, D.J., 2006, "Real-time dynamic substructuring in a coupled oscillator-pendulum system, " *Proceedings of the Royal Society A* 462, 1271–1294.

Leine, R.I., van Campen, D.H., and Keultjes, W.J.G., 2002, "Stick-slip whirl interaction in drill-string dynamics, " *Journal of Vibration and Acoustics* 124(2), 209–220.

Mihajlović, N., van Veggel, A.A., van de Wouw, N., and Nijmeijer, H., 2004, "Friction-induced torsional vibrations in an experimental drill-string system, " in *Proceedings of the 23rd IASTED International Conference,* Grindelwald, Switzerland.

Rasband, S.N., 1990, *Dynamics,* Wiley, New York, chapter "The circle map and the devil's staircase ," pp. 128–132.

Răsvan, V., Selişteanu, D., and Niculescu, S.-I., 2006, "Lossless propagation models describing the transients of combined heat/electricity generation, " in *Proceedings of the 6th IFAC Workshop on Time-Delay Systems,* L'Aquila, Italy, .

Seydel, R., 1994, *Practical bifurcation and stability analysis,* Springer, New York.

Stépán, G., 1989, *Retarded dynamical systems,* Longman, London.

Stépán, G., and Szabó, Z., 1999, "Impact induced internal fatigue cracks, " in *Proceedings of DETC'99,* Las Vegas, Nevada, USA.

Szalai, R., 2005, *PDDE-CONT: a continuation and bifurcation software for delay-differential equations,* `http://seis.bris.ac.uk/~rs1909/`.

Tucker, R.W., and Wang, C., 1999*a,* "An integrated model for drill-string dynamics, " *Journal of Sound and Vibration* 224(1), 123–165.

Tucker, R.W., and Wang, C., 1999*b,* "On the effective control of torsional vibrations in drilling systems, " *Journal of Sound and Vibration* 224(1), 101–122.

Tucker, R.W., and Wang, C., 2003, "Torsional vibration control and Cosserat dynamics of a drill-rig assembly, " *Meccanica* 33(1), 145–161.

van de Vrande, B.L., van Campen, D.H., and de Kraker, A., 1999, "An approximate analysis of dry-friction-induced stick-slip vibrations by a smoothing procedure, " *Nonlinear Dynamics* 19(2), 159–171.

Weideman, J.A., and Reddy, S.C., 2000, "A MATLAB differentiation matrix suite, " *ACM Transactions on Mathematical Software* 26(4), 465–519.